Supplemental Material

Gyral and Sulcal Contributions to Structural and Functional Connectivity in the Human Cerebral Cortex

Frithjof Kruggel, Ana Solodkin

1 Segmentation of Region Types

1.1 Segmentation of cortical features

Generation of hemispheric surfaces: Native T1- and T2-weighted structural images were linearly co-registered, corrected for intensity inhomogeneities, and the intracranial space was extracted. This space was classified into four compartments, roughly corresponding to GM, WM, cerebro-spinal fluid (CSF) and connective tissue. The inner cavities of the WM segmentation (e.g., inner ventricles, basal ganglia) were filled to form a binary object with genus zero. The cerebellum and brain stem were clipped 15 mm below the AC-PC plane, and split into hemispheres at the mid-sagittal plane. A triangulated surface was computed from this object, and optimally adapted to the GM/WM interface. These meshes retained the individual dimensions of the acquired images (≈ 0.7 mm vertex distance, about 230.000 vertices, about 0.35 mm^2 Voronoi area per vertex). Cortical thickness [6] and myelin ratio [3] were determined at each vertex location, using the intensity-corrected T1- and T2-weighted images.

Segmentation of cortical basins: Surface curvature was computed from the hemispheric mesh, represented by the shape index (Fig. SF1, top left). Geodesic depth was determined in image space, using a constrained distance transform on the sulcal compartment and interpolated at vertex positions (Fig. SF1, top right). Finally, basins were segmented by a watershed-region growing process guided by surface curvature and geodesic depth. Each basin received a unique label stored at each vertex (Fig. SF1, below left). Regions that were clipped at the mid-sagittal plane and the brain stem were excluded from the process. This procedure yielded 100-140 basins per hemisphere. Basins implicitly encode surface properties: their borders correspond to shallow cortical ridges, and centers to deep sulcal folds.

Inter-subject alignment: To compare data across individuals, each hemispheric mesh was unfolded to a unit sphere while minimizing angle and area distortion [5]. The overall correspondence between individual spherical meshes was maximized by finding a rotation that optimizes the normalized mutual information of the vertex-wise basin labels with an arbitrarily chosen reference. Finally, basin labels were re-sampled on an icosahedral mesh matching the spatial resolution of the original data (ico7, 163842 vertices; Fig. SF1, below right). Likewise, geodesic depth, curvature, cortical thickness, and myelin ratio were re-sampled at each vertex location. This process led to a spatial normalization across individuals: Each vertex was considered as homologue between

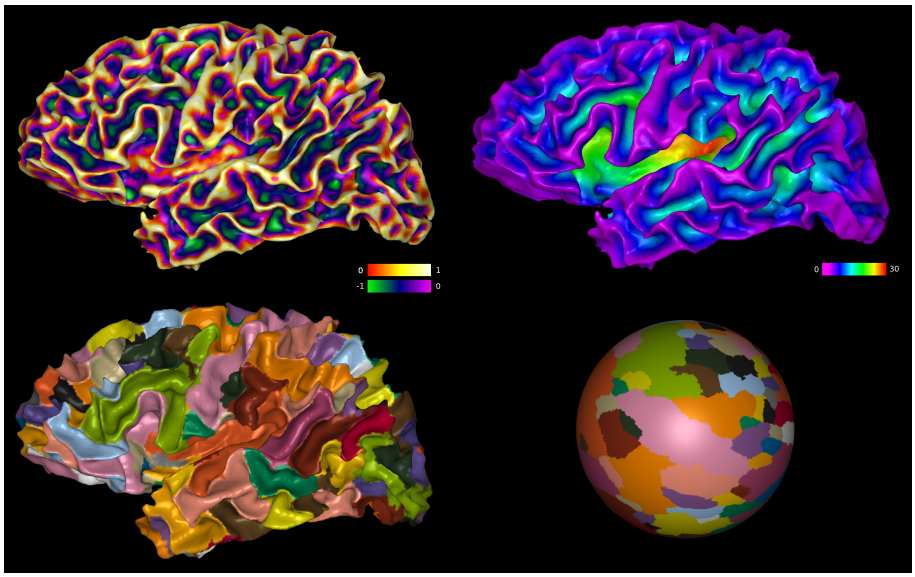

Figure SF1: Processing stages for basin segmentation: Surface shape index (top left, dimensionless units), geodesic depth (top right, in mm), basin segmentation (below left, arbitrary color labels), and aligned spherical map (below right, arbitrary color labels).

individuals. Technically, data for each hemisphere were stored as a 3D matrix of the 1051 subjects by 163842 vertices by five features, along with the spherical mesh that represented vertex positions and neighborhood relationships.

1.2 Centers of low cortical variability

If all brains had identical surface features, basin labels at each vertex would also be identical. Using the basin segmentation of an example brain as a reference, we computed a basin variability map as follows: For a reference sphere S_r with M basin labels and an object sphere S_o with N basin labels, we computed an $M \times N$ matrix $O(m, n)$ of label correspondences. Nonzero entries in row m of this matrix indicate the amount of overlap between region m in the reference and regions n on the object mesh. The row-wise maximum denotes the basin on S_o that best corresponds to basins m on the reference. For each row, we ranked column-wise entries by decreasing values, denoting the highest rank $R(1)$ as zero. For our variability metric V, we used the rank-weighted sum of region overlaps:

$$V_m = \sum_{n}^{N} R(O(m, n)) * O(m, n). \tag{1}$$

The variability is zero for a one-to-one match m to n, while any other overlapping regions increase the metric by the amount of overlap, weighted by the rank. All vertices of basin m received the variability score V_m corresponding to this basin. Using one sub-

ject as a reference, averaging the additional 1050 pair-wise variability maps resulted in an *individual* variability map.

Generally, regions of low variability map to deep sulci, while gyral crowns and rims (e.g., along the midline; along the lateral sulcus) are variable. Centers of low variabilty (CLV) were found by searching for local minima on the individual variability map (Fig. SF2, top right).

1.3 Processing of diffusion-weighted imaging data

The three B-shell series of paired L/R blip DW MR scans were corrected for subject motion and susceptibility distortions [1]. Next, voxel-wise estimates of the orientation distribution function of water motion were computed using the constrained spherical deconvolution (CSD) method [4]. Finally, tracking of fiber connections was performed via a probabilistic method [8].

Seeds for the tracking process were generated by the following procedure: The voxel-wise fractional anisotropy was estimated from the CSD data above, masked by the averaged B_0-images of the preprocessed DWI data. The high-resolution T2-weighted anatomical scan was registered with the B_0-images in DWI space. Both scans were combined and segmented using a Gaussian mixture model into four classes (roughly corresponding to compartments cerebro-spinal fluid (CSF), WM, GM, and other). The WM compartment was extracted as a binary object in voxel space. The hemispheric surface mesh with vertex-wise basin labels was adapted to this WM object using linear registration followed by nonlinear deformation. Finally, basin labels were transferred from the surface mesh to the closest voxel on the surface of the WM object. A careful assessment of the matching quality is important, in order not to bias the generation of seed voxels for tracking in sulcal vs. gyral areas. Thus we obtained a set of basin-labeled voxels on the WM/GM interface in DWI space per hemisphere. We used on average 85000 seeds per hemisphere and 100 repetitions per seed for tracking. Tracks that did not end at a labeled surface voxel were discarded. This process yielded 2-5 million tracks per hemisphere. We filtered out some spurious fibers based on a length/distance criterion, i.e., long fibers that connected two cortical areas nearby.

As a result, we obtained a set of fiber tracks, for each subject and hemisphere, connecting WM/GM surface locations with known basin labels.

1.4 Clustering of fiber connections into communities

Using fiber tracks and basin labeling, we computed hemisphere-wise fiber *connectivity matrices*: Consider subject a with n_a distinct basin labels and allocate a matrix $C(n_a, n_a)$. Increment element $C(i, j)$ if a fiber starts at basin label i and ends at basin label j. Normalize C by the number of connections. Thus, entries in this matrix represent the connection probability between regions. Subject-wise matrices were clustered using a heuristic algorithm [2], leading to 6-10 communities per subject and hemisphere (Fig. SF2, top).

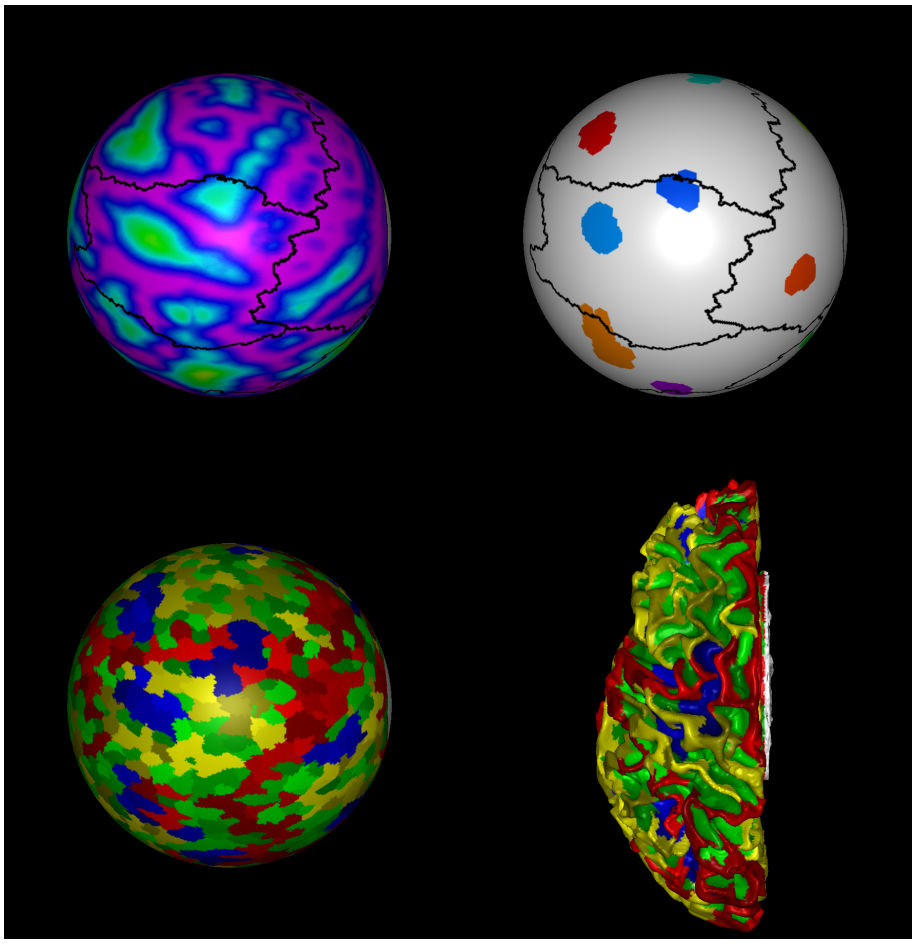

Figure SF2: Region segmentation in an example subject. Top left: Borders of fiber communities (black) overlaid onto geodesic depth (magenta: gyral crowns; green: sulci). Top right: Borders of fiber communities (black) overlaid onto centers of low variability (colored). Below left: Region segmentation into (1) border gyral regions (shades of red); (2) inner gyral regions (shades of yellow); (3) core sulcal regions (shades of blue); (4) peripheral sulcal regions (shades of green). Below right: Segmented regions mapped onto the corresponding WM/GM surface.

1.5 Segmentation of gyral and sulcal regions

An individual hemispheric surface was segmented into sulcal and gyral areas using the scale invariant shape index which is positive in concave and negative in convex regions. Peaks of gyral crowns were determined as local maxima of the shape index. Sulcal roots were determined as local minima of the shape index with a minimum geodesic depth of 5 mm (Fig. SF2, top left). Results were filtered such that peaks had a distance of at least 8 arc degrees. Starting from these peaks and roots, a curvature guided watershed region growing procedure was used to segment the hemispheric surface into the gyral and sulcal patches.

By construction, borders between fiber communities coincide with gyral ridges.

Borders were extracted and dilated on the spherical mesh to bands of 8 vertices width. Gyral patches that coincide with borders were denoted as *border gyral regions*, the others as *inner gyral regions*. As described above, the deepest sulcal roots show much less variability in space across subjects, called *centers of low variability* (Fig. SF2, top right). Thus we distinguished sulcal patches that coincide with CLVs as *core sulcal regions*, the others as *peripheral sulcal regions* (Fig. SF2, below left).

2 Definition of Network Measures

Subject-wise connectivity matrices were recomputed according to the regions obtained above. Connectivity matrices are equivalent to a weighted bidirectional network graph, in which nodes corresponds to cortical regions, and edge weights to the connection probability between regions. Regions were characterized by 9 nodal network metrics [7]:

1. *Density* d measures the cumulative probability of connections to region i, divided by the region area:
$$d_i = \sum_j^n C(i,j)/A(i) \tag{2}$$

2. *Degree* g corresponds to the number of regions connected to region i:
$$g_i = \sum_j^n C(i,j) > 0 \tag{3}$$

3. The *betweenness centrality* b denotes the fraction of all shortest paths that connect through region i:
$$b_i = \frac{1}{(n-1)(n-2)} \sum_j^n \frac{\#p_i(j,k)}{\#p(j,k)}, \tag{4}$$
where $\#p(j,k)$ is the number of shortest paths between regions j,k and $\#p_i(j,k)$ those that pass through region i. Regions with higher betweenness centrality have more control of the network.

4. *S-core decomposition:* In the graph that represents a connectivity matrix, the highest connectivity s_{max} between any two nodes was determined. All edges in the graph with a connectivity less or equal than s_{max} were removed. A level counter for all remaining nodes was increased. This process was repeated until the graph was empty. Thus the s-core of a region corresponds to its weakest connectivity in the network.

5. The *degree z-score* represents the normalized strength of a region within its community:
$$z_i = \frac{(s_i - \overline{s_j})}{\sigma(s_j)} \quad \text{with} \quad s_j = \sum_{k \in M_i} C(j,k), \tag{5}$$
where s_i corresponds to the connection strength of region i in community M_i, $\overline{s_j}$ and $\sigma(s_j)$ to the mean and standard deviation of the within community strength.

6. The *efficiency* e of a region's connectivity is computed as:

$$e_i = \frac{1}{d_i(d_i-1)} \sum_j^n \left(\frac{C(i,j)\, C(i,k)}{l(p_i(j,k))} \right)^{1/3}, \tag{6}$$

where d_i corresponds to the degree of region i and $l(p_i(j,k))$ to the length of the shortest path between regions j,k that contains only neighbors of region i. Efficiency represents the resilience at region i: How well connectivity is provided by its neighbors when it is removed.

7. The *clustering coefficient* c represents the embeddedness of a region in the network:

$$c_i = \frac{2}{d_i(d_i-1)\, C_{max}} \sum_{j,k} \left(C(i,j)\, C(j,k)\, C(k,i) \right)^{1/3}, \tag{7}$$

where d_i corresponds to the degree of region i, C_{max} to the maximum connection probability in the network, and $C(i,j), C(j,k), C(k,i)$ to the connectivity of regions with triangle connections in the one ring at region i.

8. The *small-worldness* w measures the locality of a region's connectivity:

$$w_i = \frac{c_i\, l_r}{l_i\, c_r} \quad \text{with} \quad l_i = \frac{\sum l(p_i(j,k))}{\#p_i(j,k)}, \tag{8}$$

where c_i corresponds to the clustering coefficient of region i and l_i to the average length of shortest path connecting through region i, in relation to measures of a random graph r. A smallworld topology has a high clustering and a short path length.

9. The *participation coefficient* y corresponds to the relative connection strength of region i between communities:

$$y_i = 1 - \frac{\sum_m s_m^2}{s_i^2} \quad \text{with} \quad s_m = \sum_{k \in M_m} C(i,k), \tag{9}$$

where s_m corresponds to the connection strength of region i to those in community m and s_i to the strength of region i.

Similarly, network metrics were computed for the functional correlation matrices.

References

[1] Andersson J.L.R., Skare S., Ashburner J. (2003) How to correct susceptibility distortions in spin-echo echo-planar images: Application to diffusion tensor imaging. Neuroimage 20:870–888.

[2] Campigotto R, Cespedes PC, Guillaume JL. 2014. A generalized and adaptive method for community detection. https://arxiv.org/abs/1406.2518. Accessed: April 9, 2026.

[3] Glasser M.F., van Essen D.C. (2011) Mapping human cortical areas in vivo based on myelin content as revealed by T1- and T2-weighted MRI. Journal of Neuroscience 31:11597–11616.

[4] Jeurissen B., Tournier J.D., Dhollander T., Connelly A., Sijbers J. (2014) Multi-tissue constrained spherical deconvolution for improved analysis of multi-shell diffusion MRI data. Neuroimage 103:411–426.

[5] Kruggel F. (2008) Robust parametrization of brain surface meshes. Medical Image Analysis 12:291–299.

[6] Osechinskiy S., Kruggel F. (2012) Cortical surface reconstruction from high-resolution MR brain images. International Journal of Biomedical Imaging, doi:10.1155/2012/870196.

[7] Rubinov M., Sporns O. (2010) Complex network measures of brain connectivity: Uses and interpretations. Neuroimage 52:1059–1069.

[8] Smith R.E., Tournier J.D., Calamante F., Connelly A. (2016) Anatomically-constrained tractography: Improved diffusion MRI streamlines tractography through effective use of anatomical information. Neuroimage 62:1924–1938.

3 Supplemental Tables and Figures

Data Type	Feature	PC 1	PC 2	PC 3	PC 4	PC 5
Cortical Structure	Depth	**-0.892**	0.258	-0.159	-0.201	0.067
	Curvature	**0.923**	0.058	0.114	0.265	-0.127
	Thickness	**0.730**	0.429	-0.252	0.056	-0.302
	Myelin	0.633	0.504	-0.312	-0.022	-0.294
Structural Connectivity	Density	0.183	**0.933**	0.105	0.074	-0.147
	Degree	0.059	**0.905**	-0.275	0.076	-0.187
	Betweenness	0.044	**0.892**	-0.310	-0.021	-0.227
	S-core	-0.008	**0.740**	0.242	0.127	-0.159
	Deg. z-score	0.214	**0.813**	0.348	0.209	-0.057
	Efficiency	0.117	0.045	**0.922**	0.030	0.095
	Clustering	0.114	-0.390	**0.839**	0.013	0.165
	Small-worldness	0.100	0.088	**0.797**	0.095	0.002
	Participation	0.055	**0.740**	-0.450	0.009	-0.283
Functional Connectivity	Density	0.635	0.164	0.125	**0.705**	0.003
	Degree	0.576	0.174	0.122	**0.734**	-0.132
	Betweenness	0.591	0.425	-0.041	0.330	-0.477
	S-core	0.105	0.069	-0.003	**0.751**	0.306
	Deg. z-score	0.550	0.044	0.194	**0.749**	0.044
	Efficiency	0.086	-0.098	0.067	0.181	**0.915**
	Clustering	-0.326	-0.224	0.016	-0.065	**0.888**
	Small-worldness	-0.335	-0.246	-0.099	0.141	**0.739**
	Participation	-0.042	0.400	-0.189	0.020	-0.657
	Variance	0.249	0.228	0.132	0.098	0.144

Table ST1: Right hemisphere: Factor loadings of PC scores for cortical, structural and functional connectivity features. These components represented 84.9% of the overall variance. Loadings $> |0.7|$ were shown in bold. Component 1 loaded onto cortical features, component 2 onto the integrative properties of structural connectivity, component 3 onto segregative properties of structural connectivity, component 4 onto integrative properties of functional connectivity, and component 5 onto the segregative properties of functional connectivity.

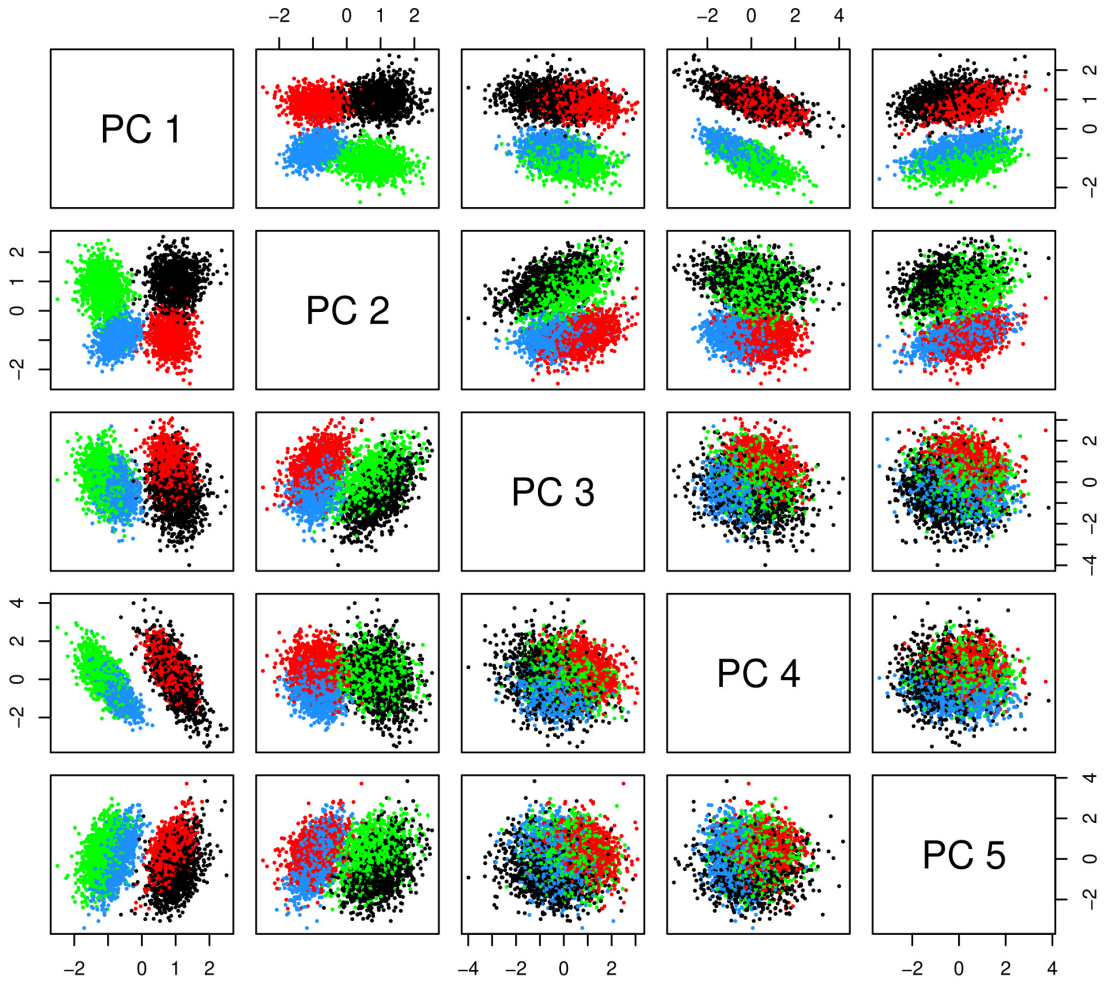

Figure SF3: Right hemisphere: Scatter plot of PC scores. Each dot corresponds to component scores for one feature vector, sampled in peripheral (blue) and core (green) sulcal regions, inner (red) and border (black) gyral regions. Components represented: (1) cortical features; (2) integrative and (3) segregative properties of structural connectivity; (4) integrative and (5) segregative properties of functional connectivity.

Data Type	Feature	Border Gyri		Inner Gyri		Core Sulci		Peripheral Sulci	
		Rank	p-value	Rank	p-value	Rank	p-value	Rank	p-value
Cortical Structure	Depth					L < R	<1e-4	L > R	<1e-4
	Curvature	L < R	<1e-4	L < R	<1e-4	L > R	<1e-4	L > R	5.55e-3
	Thickness	L < R	<1e-4	L < R	<1e-4	L < R	<1e-4	L > R	<1e-4
	Myelin			L < R	<1e-4	L < R	<1e-4	L > R	<1e-4
Structural Connectivity	Density	L > R	<1e-4	L < R	<1e-4			L < R	1.56e-4
	Degree	L > R	<1e-4	L > R	<1e-4	L > R	<1e-4	L > R	<1e-4
	Betweenness					L < R	<1e-4	L > R	<1e-4
	S-core	L > R	<1e-4						
	Deg. z-score	L > R	<1e-4	L < R	<1e-4	L > R	<1e-4	L < R	<1e-4
	Efficiency	L < R	<1e-4	L < R	<1e-4	L < R	<1e-4	L < R	<1e-4
	Clustering	L < R	1.39e-2	L < R	<1e-4	L < R	4.69e-4	L < R	<1e-4
	Small-worldness			L < R	<1e-4	L < R	<1e-4	L < R	<1e-4
	Participation			L > R	<1e-4	L < R	<1e-4	L > R	<1e-4
Functional Connectivity	Density	L > R	<1e-4	L < R	<1e-4	L > R	<1e-4		
	Degree	L > R	<1e-4	L < R	<1e-4				
	Betweenness	L > R	1.28e-4	L < R	<1e-4	L < R	<1e-4	L > R	<1e-4
	S-core								
	Deg. z-score	L > R	<1e-4					L < R	1.82e-2
	Efficiency	L > R	6.23e-3	L > R	<1e-4	L > R	<1e-4		
	Clustering					L > R	<1e-4		
	Small-worldness					L > R	<1e-4		
	Participation					L < R	<1e-4	L > R	<1e-4

Table ST2: Asymmetry of cortical, structural and functional connectivity features, separated by region type. The symbol $>$ denotes a significant left-ward difference (paired t-test, after Bonferroni correction).

Data Type	Feature	Side	Border Gyri		Inner Gyri		Core Sulci		Peripheral Sulci	
			Rank	p-value	Rank	p-value	Rank	p-value	Rank	p-value
Cortical Structure	Depth	L	F > M	<1e-4	F > M	<1e-4			F > M	<1e-4
		R	F > M	<1e-4	F > M	<1e-4	F > M	1.16e-2	F > M	<1e-4
	Curvature	L	F < M	<1e-4	F < M	<1e-4				
		R	F < M	<1e-4	F < M	<1e-4				
	Thickness	L			F > M	2.02e-2	F > M	<1e-4	F > M	<1e-4
		R			F > M	2.75e-3	F > M	<1e-4	F > M	<1e-4
	Myelin	L	F > M	2.77e-2	F > M	<1e-4	F > M	<1e-4	F > M	<1e-4
		R			F > M	<1e-4	F > M	<1e-4	F > M	<1e-4
Structural Connectivity	Density	L	F < M	1.53e-2			F > M	2.32e-3		
		R								
	Degree	L	F < M	7.59e-4						
		R								
	Betweenness	L								
		R								
	S-core	L								
		R								
	Deg. z-score	L	F < M	1.11e-2			F > M	<1e-4		
		R	F < M	7.99e-3						
	Efficiency	L					F > M	<1e-4		
		R								
	Clustering	L					F > M	4.07e-2		
		R								
	Small-worldness	L					F > M	4.54e-2		
		R								
	Participation	L								
		R								
Functional Connectivity	Density	L	F > M	<1e-4	F < M	3.14e-2				
		R	F > M	9.22e-4						
	Degree	L	F > M	<1e-4						
		R	F > M	1.07e-3						
	Betweenness	L	F > M	7.01e-3						
		R	F > M	8.26e-3						
	S-core	L								
		R								
	Deg. z-score	L	F > M	<1e-4	F < M	<1e-4				
		R	F > M	<1e-4	F < M	<1e-4				
	Efficiency	L								
		R								
	Clustering	L								
		R								
	Small-worldness	L								
		R								
	Participation	L								
		R								

Table ST3: Sex-related differences of cortical, structural and functional connectivity features, separated by region type. The symbol > denotes significantly higher scores in females (t-test, after Bonferroni correction).